Computer Assisted Methods in Engineering and Science
29(3): 261–292, 2022, doi: 10.24423/cames.523

Determining Frequency-Energy Dependency of Nonlinear Normal Modes and Internal Resonances Using a Numerical Independent Approach

Arash GHARIBLOU*, Mussa MAHMOUDI

Department of Structural Engineering, Faculty of Civil Engineering, Shahid Rajaee Teacher Training University, Tehran, Iran; e-mail: m.mahmoudi@sru.ac.ir

* *Corresponding Author e-mail: ghariblou@sru.ac.ir*

Application of linear normal modes to the nonlinear area provides an in-depth investigation of structures. In this paper, a straightforward approach is proposed to investigate nonlinear normal modes (NNMs) thoroughly and focus on all possible solutions and bifurcations, independent of all initial assumptions and prior solutions. In this context, after discretization of the response domain over an appropriate resolution, a periodicity algorithm is suggested to capture the solutions that meet the NNMs criteria. Afterward, the frequency and energy of the system during accepted responses and degrees of freedom (DOFs)' relations are derived. Finally, after verifying the proposed approach and acquiring new internal resonances, the frequency-energy plots and NNMs of a nonlinear elastic system with more substantial nonlinearities and a two-story steel structure with nonlinear material are studied. It is worth noting that the periodicity algorithm and capturing all possible solutions and bifurcations are among the apparent novelties of the current paper.

Keywords: nonlinear normal modes, frequency-energy dependency, independent approach, internal resonances, bifurcations, nonlinear dynamic analysis.

1. Introduction

Any attempt to apply traditional linear analysis to obtain real-world nonlinear systems, at best, contributes to suboptimal analyses, which cannot meet the demands of new developments and modern achievements efficiently. One of the most prominent and physically meaningful mathematical approaches is applying eigenvalue and eigenvector concepts to motion equations of linear problems, known as natural frequencies and linear normal modes (LNMs), respectively. Expanding these concepts to nonlinear motion equations, even with a continuously-

changing stiffness matrix, fails at finding NNMs and their corresponding continuously-changing frequencies. This is because, in such problems, NNMs are curves (and no longer straight lines), and a linearized method cannot be used to satisfy nonlinear complexities. In this context, extending LNMs to NNMs requires an in-depth conceptual relationship between them, which could be met through a joint basic definition based on one of their common properties. Among them, the *superposition principle*, which allows obtaining any final solution of an excited conservative linear system from a linear combination of LNMs [8], and *orthogonality*, which means that the product of two different LNMs in the phase space is always equal to zero [21], are not applicable to the nonlinear area.

However, beyond familiar linear concepts, facing *bifurcations* in the frequency-energy subspace [5] could provide a situation of exchanging energy between two separate NNMs, known as *internal resonance* [17, 41], which could trigger the *number of NNMs* to exceed the number of DOFs [11, 18]. It is worth mentioning that these modal interactions do not have any linear counterpart and usually occur when harmonics of responses resonate with each other. In contrast, *invariance* is a joint concept between both LNMs and NNMs and relies on the fact that if the motion is initiated coincidently on one mode, the other modes remain off during the oscillation [27]. In this context, the *vibration-in-unison* as a joint concept between LNMs and NNMs is employed to form the basic definition of NNMs by Rosenberg [28] to pave the way for linking all DOFs to a master DOF, and by extending the borders of this definition, several analytical and numerical techniques were developed to calculate NNMs.

From an engineering viewpoint, all the theoretical investigations can be justifiable in the circumstances of proper applications. As the concept of NNMs can cover a vast portion of nonlinear areas, and their linear counterpart as a familiar subject paved the way for a deep conceptual understanding of this concept, engaging in such a rich field of study could contribute to determining unknowns of the nonlinear realm. In this context, NNMs can be used to form reduced-order models (ROMs) [23, 32], modal analysis [19, 42], damage detection [2, 33], and extract the modal characteristics [20, 35, 40]. Besides, some interesting real-world case studies such as the investigation of an F-16 aircraft [6, 22], nonlinear rotordynamics of mechanical rotary systems [3], rubble-pile asteroids [4], rail track systems [7, 10], wind turbines [42], and nonlinear dynamics of bridges [1] have been presented recently to investigate their nonlinear dynamics through normal modes.

However, considering uncertainties of NNMs besides the complexities of the current approaches and their dependencies on some assumptions, especially taking LNMs as the starting point and only following their continuous path, sparked the idea of an independent approach to investigate NNMs thoroughly without

any initial assumption, which satisfies the basic definition of NNMs independently. In this paper, a domain-based approach is proposed to investigate all NNM candidates thoroughly and pays a great attention on all possible solutions. To this end, after discretizing the response domain through an appropriate resolution, numerical integration techniques are employed to obtain motion equations responses. Afterward, a novel algorithm is proposed to check the resulting response's periodicity and subsequently calculate the frequency of the periodic ones. Based on that, the relation between displacements and velocities of DOFs with respect to the others and the system's total energy during each periodic solution ate stored and used to form NNMs and frequency-energy plots (FEPs). Finally, after verifying the proposed approach over a well-known problem with nonlinear geometry and finding some new internal resonances, the FEPs, *quasi*-continuous demonstration of NNMs over energy, and the relation of DOFs in phase space of a system with nonlinear elastic materials and large deformations [38] are presented.

Although previous methods have calculated NNMs with high precision, the objective of the present paper is to introduce a new independent and straightforward point of view toward NNMs. Meanwhile, the suggestion of a novel algorithm for checking the periodicity of responses without a need of the period time as input (such as shooting technique) and producing that as an output, its ability to find all possible responses, bifurcations, and their corresponding internal resonances are among the novelties of the current paper. It is worth noting that applying the independent approach with low resolution as a complement tool could provide a valuable framework to verify other methods' results quickly, and employing higher resolutions contributes to observing all periodic solutions independent from starting point and bifurcations difficulties during a more significant amount of time, which seems inevitable in the face of uncertainties. In the following sections, first, the foundations of the NNMs concept and the procedure of the proposed independent approach ranging from periodicity algorithm to evaluation of the system's total energy, are discussed in Sec. 2. Afterward, the proposed approach is applied to a known system to validate the whole procedure in Sec. 3. Finally, the FEPs and NNMs of a nonlinear elastic system with more substantial nonlinearities and a two-story steel structure with nonlinear materials are illustrated in Sec. 4 and discussed in Sec. 5.

2. Nonlinear normal modes

2.1. Definitions

Theoretical advances in nonlinear sciences formed the concept of NNMs, pioneered by Rosenberg [29]. Rosenberg extended LNMs of conservative systems to

the nonlinear area and, based on that, defined NNMs as the relation between different DOFs during "vibration in unison" of the system (i.e., synchronous oscillations), which relies on the fact that all DOFs have an equal period during vibration and thus reach their extremum and zero positions simultaneously. Through this definition, each DOF can be expressed as a function of other DOFs. Therefore, by taking one of them as the "master" coordinate, all the other DOFs can be defined as dependent variables. The relations between each two DOFs (the mentioned functions) are called "modal curves," which are nonlinear. If special spatial symmetries exist, this concept can be simplified to straight modal lines, in which the NNM is called similar. As discussed in [11], this definition suffers some restrictions and does not contribute to all desired points. To this end, an extended version definition of "non-necessarily synchronous periodic oscillations" was proposed, which constructs the NNMs from periodic responses even with non-equal period values at each DOF.

The periodic-based nature of Rosenberg's definition made it restricted to the conservative systems. So, the necessity of a modified definition for non-conservative systems made Shaw and Pierre generalize the previous one [30]. The authors considered an NNM as a 2-D invariant manifold in phase space. The mentioned manifold passes through a stable equilibrium point, where the corresponding LNM passes through it too, but with the geometry of a plane, and the nonlinear manifold's curve is tangent to the LNM's plane at that point. This definition has a more general concept as it is applicable to both damped and undamped systems. In recent years, Krack [14] proposed a novel definition suited to systems under external harmonic excitation and negative linear damping, which relies on adding a damping term with the required sign and magnitude to the process of checking periodicity. Finally, although various definitions exist in the literature, NNMs have a unique conceptual foundation, and in the case of each problem, a compatible definition should be adopted. In this context, since the existing knowledge of damping mechanisms suffers many restrictions, the design process used in the industry, even in linear systems, is usually based on conservative systems. Thus, in this paper, NNMs are considered as the relation of DOFs during non-necessarily synchronic periodic oscillations.

2.2. Methodology

Among many calculation techniques, *analytical-based methods*, as pioneering ones, could be categorized into different classes. The first method uses an *energy-based formulation* to obtain NNMs by defining NNMs as certain functions of the relationship between displacements of slave DOFs and a master DOF to eliminate time derivations from the equations of motion and calculate the de-

sired functions [13]. The next popular approach is based on the *invariant manifold technique*, which closely resembles the previous energy-based formulation and tries to eliminate explicit time dependence. In this context, a pair of displacement and velocity are taken as master coordinates, the remaining variables as slaves to them to approximate a local solution using polynomial expansion of those master coordinates [31]. The *Multiple scales method* is a perturbation method that has received considerable attention in calculating NNMs. It attacks governing differential equations directly and attains the solution in the form of an asymptotic expansion over transformed motion equations through a small non-dimensional parameter [16].

On the other hand, attaining exact analytical solutions for many nonlinear and complex motion equations seems very expensive and even impossible. So, the arrival of computers paved the way for calculating approximate solutions and solving nonlinear problems through *numerical methods*. The *harmonic balance method* could be considered a semi-analytical approach, based on the expansion of the unknowns and parameterized through a finite Fourier series and frequency-domain approaches to find NNMs [9]. Surprisingly, there have been few attempts to employ numerical methods in calculating NNMs. In this regard, implementing both the multiple scales and the invariant manifold approach and applying them to finite element models is another efficient numerical approach for obtaining NNMs of non-conservative systems [15, 26]. The part-by-part continuation of periodic solutions is called *sequential continuation*. Combining this concept with a *shooting technique* contributed to an approach to solve the nonlinear boundary value problem numerically, which resulted in a family of NNMs and has received considerable attention recently [34, 36, 39].

All the mentioned numerical techniques are based on some initial assumptions; especially, they usually take the LNMs as starting point and follow their continuous path. Besides, Lyapunov [18] proved that the number of DOFs is the minimum possible number of modes, and in the case of NNMs, this number can exceed that value, which increases the uncertainty about finding all possible answers through the existing approaches. This uncertainty highlights a need for a thorough domain-based approach in order to investigate all possible solutions. To this end, a straightforward approach was proposed, which tries to eliminate the dependence of the process on the starting point, step-size-based convergence, and other initial assumptions. So, the present study's primary aim is to find all possible responses in a discretized manner that satisfying the NNMs criteria in the general system (1) under undamped free vibration. So, initially, a proposed algorithm to capture accepted points based on the adopted definition of NNMs is discussed, which in contrast to the Shooting Technique, does not require the frequency value as input and calculates the frequency of periodic responses independently. Afterward, the whole process of finding NNMs, including assigning

resolution to the domain, numerical integration details, and total energy calculation, is presented:

$$[M]\{\ddot{x}(t)\} + [K]\{x(t)\} + \{f_{nl}(x(t))\} = 0, \tag{1}$$

where x and $\ddot{x}$ are displacement and acceleration vectors, K is the corresponding linear stiffness matrix, M is the mass matrix, and f_{nl} is the nonlinear restoring force vector.

2.2.1. NNMs criteria. The first step is to specify the basic definition of the NNMs problem and develop a path to apply the adopted definition numerically. In this context, Rosenberg's initial definition cannot cover the situations in which each DOF of a system vibrates periodically, and the oscillation frequencies of different DOFs are not equal, such as during internal resonance. Besides, the lack of knowledge about damping mechanisms contributes to the fact that real-world structural designs are usually based on conservative systems. So, the previously mentioned extended version of Rosenberg's definition of *non-necessarily synchronous periodic oscillations of conservative systems* is employed in this study as the criterion of being an NNM. In other words, all the initial conditions of the system (1) that contribute to periodic answers are taken as desired points, even if each DOF has a different period value (T).

To this end, a procedure for evaluating motion responses is necessary to check its periodicity as the confirmation filter. In this context, the most pervasive approach is the shooting technique, which takes the period value, namely T, as input and checks if the residual of the response between zero and T time is less than the accepted error or not. So, an initial guess is required for T, produced from the T of previous continuous solutions in other methods. However, this dependency on an initial assumed T makes the Shooting Technique inappropriate to be a powerful independent NNM-finder tool. In this paper, an alternative algorithm is suggested to check the periodicity of the given response, and then if the NNMs criteria are satisfied, the corresponding period time of that solution is found. Finally, a step-by-step procedure is presented below to explain the proposed filter in detail, and Fig. 1 shows a graphical demonstration of the mentioned steps in one of the DOFs at one point corresponded with the system (5), excited with initial values of $x_1(0) = 1.34$, $x_2(0) = 17.05$ at zero time under undamped free vibration.

A step-by-step procedure is as follows:

1. Find all peaks of the response, which could be met through the *findpeaks* command in MATLAB or consider all local maximums in the whole response [37].

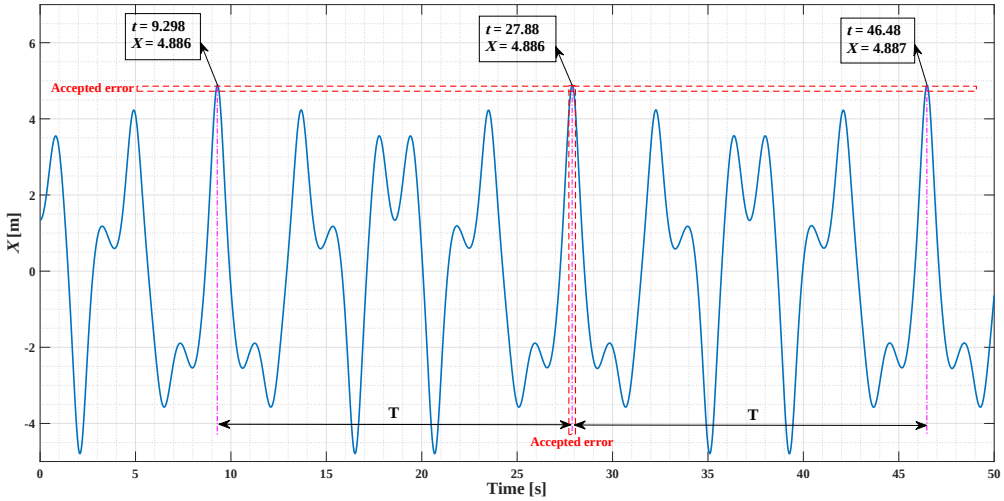

FIG. 1. Graphical demonstration of applying NNMs criterion to x_1 of a point with $(x_1(0) = 1.34,\ x_2(0) = 17.05)$.

2. Among them, find the absolute peaks, in which their difference with the largest absolute amount of the response, namely maximum (x), is less than an accepted error value. This value is calculated by multiplying a user-defined coefficient as the "accepted error percentage (ε_p)" to maximum (x). The use of percentage value as an accepted error instead of a constant value is due to increasing the applicability of the same algorithm to different problems with different scales of numbers.
3. If the number of absolute peaks exceeds three, the difference between the time of the first and second ultimate peak should be compared to the corresponding value of the third and second ultimate peak.
4. If the discrepancy between the first and second interval of time is less than the accepted value for error, the response is periodic, and its period is equal to the mentioned interval of time. Here again, the accepted error value for time is calculated by multiplying the user-defined coefficient as the "accepted error percentage (ε_t)" by the first time interval.
5. Continue steps 1 to 4 for all DOFs.
6. If all the DOFs have periodic motions, regardless of equal periods or not, the initial conditions that cause these responses are passed through the NNMs criteria filter.

2.2.2. Body of process. All previous numerical methods start their continuous process from an initial point arising from LNMs. In addition to their ad-

vantages, since NNMs' numbers could exceed the number of DOFs [11] and there is no proven upper bound for it, a question remains unanswered: do the previous methods' results cover all possible answers? By accepting a standard definition for conservative systems, eliminating all the restrictive assumptions is the first step in answering this question and having a thorough analysis. So, the only way to eliminate the dependence on initial points is to evaluate all potential points. In this context, first, the continuum domain of the problem should be determined and discretized by defining a response *resolution*, which means dividing the variables domain into an adequate number of elements and transforming a continuum domain into a discretized calculable one. The more significant number of parts is taken, the higher accuracy can be obtained. By contrast, higher resolution means more calculation expenses and more accurate responses. After applying a balanced resolution and crossing variables to each other, all candidate solutions are prepared and ready to be analyzed.

As mentioned before, each potential point includes initial excitation values for each DOF as their initial conditions to solve the undamped free-response of motion equations (ODEs). Afterward, to check every point's competency, a *numerical integration* approach is required to solve the system of differential Eq. (1). In this context, MATLAB's built-in *ode45* and *ode15s* commands pave the way for a simple numerical integration far from the complexity of applying other methods based on the explicit Runge–Kutta formulation Dormand–Prince pair. To define the system of differential equations corresponding to the current problem, the ODE solvers require a transformation from second-order to first-order ODEs ($\{y'\} = f(t, y)$). In this context, by defining z as the state vector (2), including the mentioned candidate solutions, and recasting the system (1) into the state space (3), the required prerequisite of the ODE solver is met:

$$z = \begin{Bmatrix} \{x\} \\ \{\dot{x}\} \end{Bmatrix}_{2n*1}, \tag{2}$$

$$\dot{z} = g(z) = \begin{Bmatrix} \{\dot{x}\} \\ \{\ddot{x}\} \end{Bmatrix}_{2n*1} = \begin{Bmatrix} \{\dot{x}\} \\ -[M]^{-1}\left[[K]\{x(t)\} + \{f_{nl}(x(t))\}\right] \end{Bmatrix}_{2n*1}, \tag{3}$$

where n indicates the number of DOFs, x indicates displacements, $\dot{x}$ indicates velocities and $\ddot{x}$ indicates accelerations corresponding with DOFs of the system (1). Another required user-defined value is the time interval of integration, namely *tspan*, which determines the integration's start and finish time. Relative error tolerance, namely *RelTol*, is a positive scalar value and measures the rela-

tive error concerning the magnitude of each solution component. Absolute error tolerance, namely *AbsTol*, determines ignorable values of the solution, which is a positive scalar or vector with the same size as the solution. Taking e as the error of the i-th iteration of the ODE solver, it would be an acceptable error if it satisfies the condition given in (4). In stiffed problems, the *ode15s* command can be used too, but in most cases, the previously mentioned version meets all the demands:

$$|e(i)| \leq \max\left(RelTol * abs(y(i)),\ AbsTol(i)\right). \tag{4}$$

As a candidate is selected after the segmentation of the domain, its corresponding response can be obtained using the mentioned numerical integration process, and its competency to be an NNM can be checked by NNMs criteria (Subsec. 2.2.1). It is worth noting that after stimulating the system (1) based on assigning initial displacement and velocity to each DOF and solving the corresponding ODEs through the numerical integration process, the response of each DOF is a diagram with displacements on the y-axis and time on the x-axis. By assuming a synchronous vibration for a periodic response, the period time of all DOFs will be equal, and consequently, their peaks will coincide. In this context, starting the periodic response from each point on the diagram will contribute to the same response, and this sparks the idea of making all velocities equal to zero and starting the response from a peak in all DOFs, which reduces the independent variables significantly. However, as mentioned in Subsec. 2.1, in some situations, such as during internal resonances, the responses would be non-synchronic, and the period time of each DOF's periodic response would be different from the others. In this case, the peaks will not occur simultaneously, and applying zero value to all initial velocities will impose a latent restriction on the final outcoming NNMs. In conclusion, although assigning zero values to initial velocities during low energies (around LNMs) will not affect the results, they should be checked for non-zero values in higher energies, and one of the DOFs' initial velocities is valid to be considered equal to zero.

If all filters of being an NNM are passed, the next step is to calculate the current energy of that NNM. Potential and kinetic energy form the total energy of a system, and as the system is conservative, this value remains constant during the whole motion. The potential energy can be calculated by integrating the stiffness function of each spring and then combining them altogether. In the case of kinetic energy, the corresponding energy can be found based on Newton's law by integrating the inertia force, which contributes to $0.5m_i\dot{x}_i^2$, regardless of its linear or nonlinear stiffness. Figure 2 shows all the mentioned steps of the proposed algorithm briefly in a flowchart.

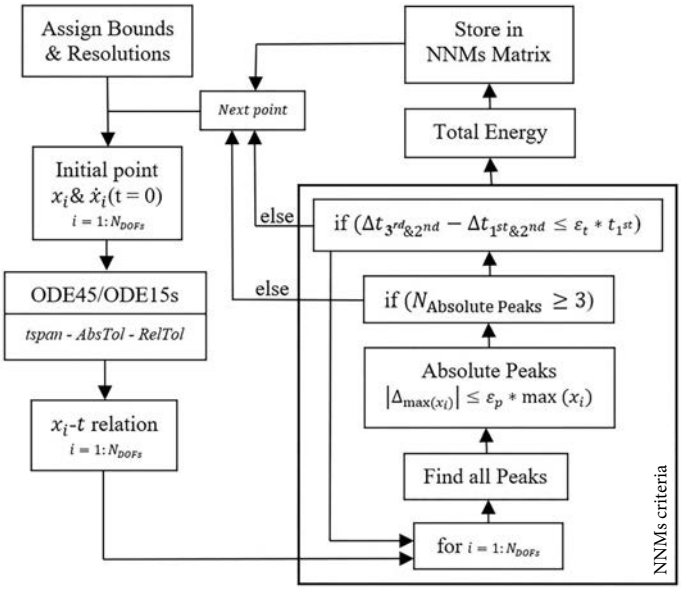

FIG. 2. Flowchart of the proposed algorithm.

3. VERIFICATION

3.1. A known nonlinear system

The *pseudo-arc length sequential continuation* method is one of the most prevalent approaches in this field of study, confirmed by experimental investigations [24]. Hence, a well-known undamped mechanical system with cubic nonlinearities evaluated in [25] is adopted, and the suggested approach is applied to that to validate its corresponding results and search for new bifurcations. The mentioned system is shown in Fig. 3, and its governing motion equations are presented in Eq. (5):

$$\begin{bmatrix} 1 & 0 \\ 0 & 1 \end{bmatrix} \begin{Bmatrix} \ddot{x}_1 \\ \ddot{x}_2 \end{Bmatrix} + \begin{bmatrix} 2 & -1 \\ -1 & 2 \end{bmatrix} \begin{Bmatrix} x_1 \\ x_2 \end{Bmatrix} + \begin{Bmatrix} 0.5x_1^3 \\ 0 \end{Bmatrix} = 0, \tag{5}$$

where x and $\ddot{x}$ indicate the corresponding displacement and acceleration of each DOF, respectively. It is worth mentioning that in small values of x, the impact of the term x^3 on response is ignorable, and by eliminating the nonlinear restoring force vector from the motion equations (5), familiar motion equations of a linear system emerge. In this context, by solving the linear eigenvalue problem, two LNMs and their corresponding natural frequencies could be obtained through the *eig* command in the MATLAB framework to check if the nonlinear system's response during low energy values is compatible with them.

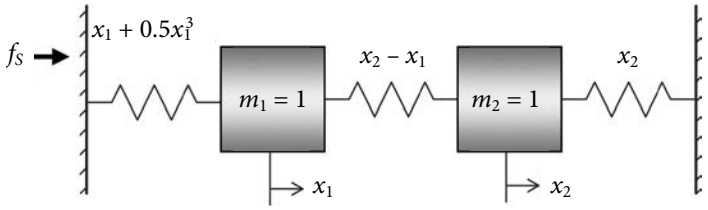

FIG. 3. Schematic representation of the studied undamped nonlinear system.

In particular, assigned values for evaluating the system (5) are presented. Initially, the upper and lower bounds of both initial x_1 and x_2 were taken equal to -20 and $+20$ with a balanced resolution equal to 0.01. Moreover, the initial value assigned to $\dot{x}_1$ is set to zero, and the bounds of $\dot{x}_2$ at zero time cover from -100 to $+100$ with a resolution of 0.05. By crossing mentioned values and working on each point separately, the domain is discretized and x_1, x_2, $\dot{x}_1$ and $\dot{x}_2$ of each point as initial values for numerical integration of governing ODEs under free vibration motion are determined. Regarding numerical integration, the desired interval for numerical integration and, consequently, for each point's response, namely *tspan*, is from $t = 0$ to 100 seconds. Furthermore, relative error tolerance, namely *RelTol*, is taken equal to 10^{-6} and absolute error tolerance, namely *AbsTol*, is taken equal to 10^{-9}. The value for both the accepted error of peaks, namely ε_p, and the accepted error of periods, namely ε_t, was taken equal to 0.1% (0.001). To prepare the previously mentioned ODEs (5) for the *ode45* command of MATLAB, Eq. (6) shows the required transformation and the expected answer after applying *ode45* at each step of numerical integration:

$$\dot{z} = \begin{Bmatrix} \dot{x}_1 \\ \dot{x}_2 \\ \ddot{x}_1 \\ \ddot{x}_2 \end{Bmatrix} \Rightarrow \begin{Bmatrix} \dot{z}_1 \\ \dot{z}_2 \\ \dot{z}_3 \\ \dot{z}_4 \end{Bmatrix}$$

$$= \begin{Bmatrix} \dot{x}_1 \\ \dot{x}_2 \\ \dfrac{-1}{m_1}(2x_1 - x_2 + 0.5x_1^3) \\ \dfrac{-1}{m_2}(2x_2 - x_1) \end{Bmatrix} \xrightarrow{ode45} \begin{Bmatrix} x_1 \\ x_2 \\ \dot{x}_1 \\ \dot{x}_2 \end{Bmatrix} \text{ over } t \text{ at } i\text{-th point.} \quad (6)$$

Regarding the frequency-energy dependency of the system (5), the corresponding value for the period time of periodic solutions will result from the

periodicity algorithm, and the total energy of those responses could be met through the sum of kinetic and potential energies. Since the studied system is conservative, the total energy is a constant value during all motion. So, in the current problem, the total energy of periodic solutions has been calculated at the zeroth time of motion. In this context, each mass kinetic energy can simply be calculated by integrating the $m\ddot{x}_i$ term, which results in $0.5m_i\dot{x}_i^2$ for each mass. Moreover, the potential energy in Fig. 3 directly stems from the absorbed energy in each spring, and regardless of compression of tension, their corresponding absolute values should be added together. Considering x_1, (x_2-x_1), and x_2 as displacement of the left, middle, and right springs, respectively, the total energy of the system (5) can be calculated from (7):

$$\text{Total energy} = \overbrace{0.5m_1\dot{x}_1^2 + 0.5m_2\dot{x}_2^2}^{\text{Kinetic energy}} + \overbrace{\int \left(k_1x_1 + 0.5x_1^3\right) dx_1 + \int \left(k_2(x_2 - x_1)\right) d(x_2 - x_1) + \int (k_3x_2)dx_2}^{\text{Potential energy}}. \quad (7)$$

3.2. Results

To validate, the proposed approach with the mentioned calculation constants is applied to the system (5) studied in [25]. In this context, Fig. 4 shows the

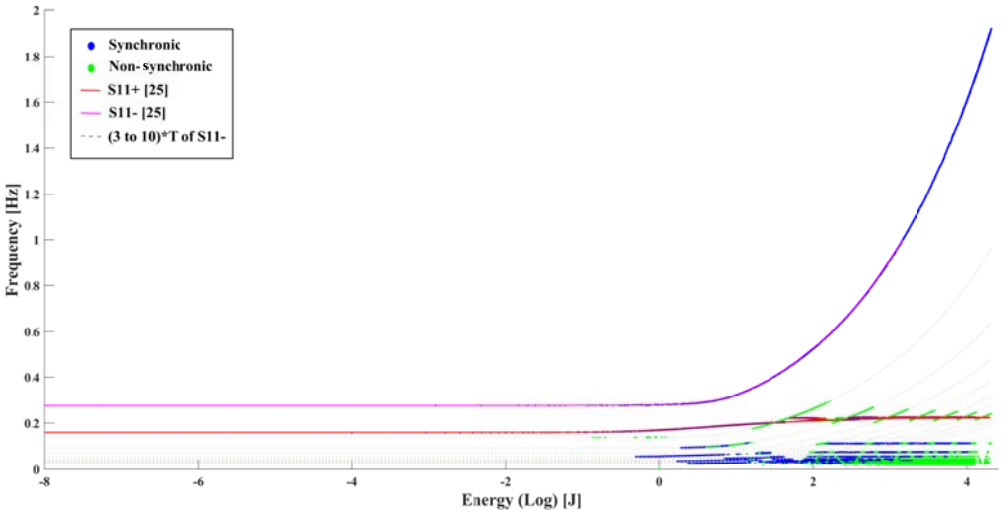

FIG. 4. Verification of the independent approach through FEP.

whole system's FEP. In this context, the previous studies' results [25] are drawn as solid lines, where a great agreement between current and previous results is evident. The upper purple curve is the extension of out-of-phase LNM, which means that the signs of initial displacements at the zeroth time are opposite, and subsequently, DOFs move in opposite directions. It is called $S11-$ where the S letter comes from the symmetrical trait of periodic motion, and U is commonly used for unsymmetrical ones. Besides, the negative sign indicates out-of-phase motion, while a positive sign is required for in-phase ones. A periodic solution with a period equal to T is still periodic under a period equal to multiples of T. So, the numbers in front of the letter are employed to show which coefficient of the primary response is running and, in the case of internal resonances, to show the origin and destination NNMs, in which the energy exchange occurs. Dash lines of FEP are multiplications of base $S11-$ based on different multiples of T. It is worth noting that the horizontal line in the starting part of NNMs agrees with the constant value for the natural frequency of LNMs, and the ascending trend of the response is due to the hardening behavior of geometrical nonlinearity, which is latent in motion equations of the system (5).

The points near multiplications of both in-phase and out-of-phase paths would face an energy exchange known as internal resonance. This phenomenon is a unique consequence of nonlinear analyses, which cannot be found in their linear counterparts. To have a closer look at different parts of the presented FEP, the close-up of the first bifurcation is illustrated in Fig. 5, where the unstable points are displayed as black dash lines, and the main stable points of the first internal resonance are captured appropriately.

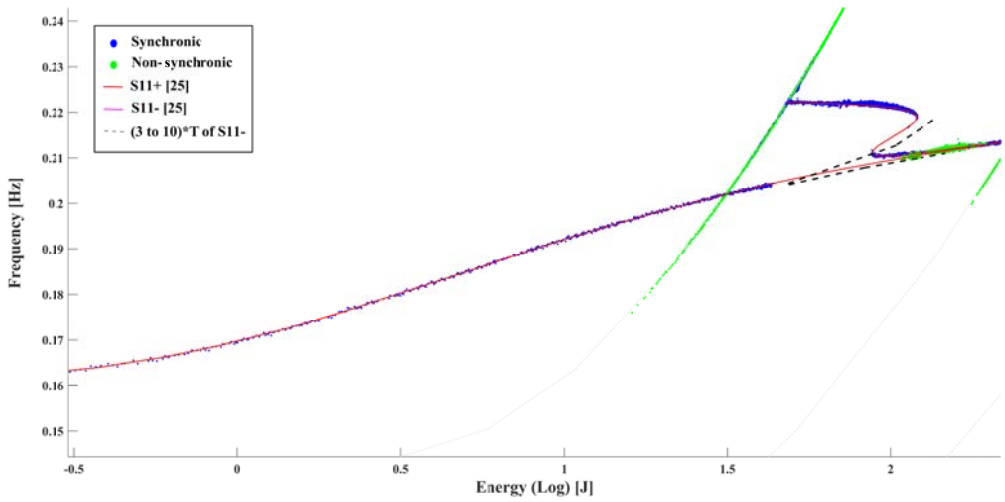

Fig. 5. Close-up presentation of the first internal resonance.

3.3. New internal resonances

Investigation of lower parts of FEP is practically impossible due to the little distance between the points, where the occurrence of internal resonances is highly probable. To this aim, the FEP was converted to a period-energy plot and is shown in Fig. 6.

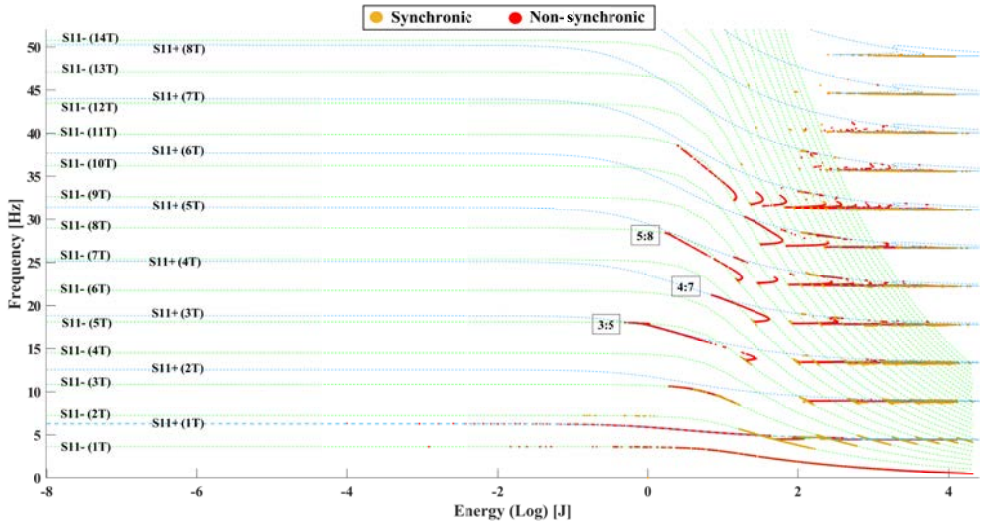

FIG. 6. Period-energy plot of the system (5).

Dash lines are multiplications of both $S11+$ and $S11-$, and the occurrence of some new internal resonances between them is salient. Again, to have a closer look at them, Fig. 7 illustrates two of them in detail.

a)

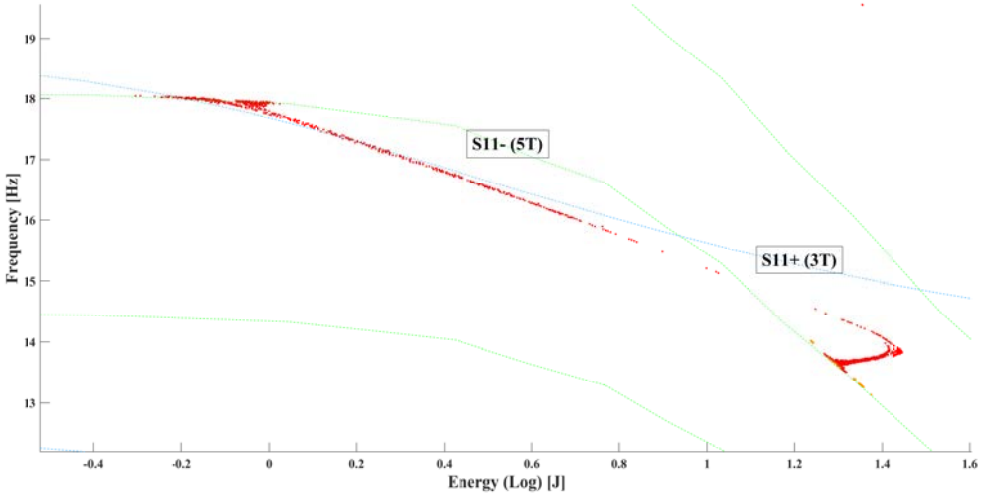

[FIG. 7a]

b)

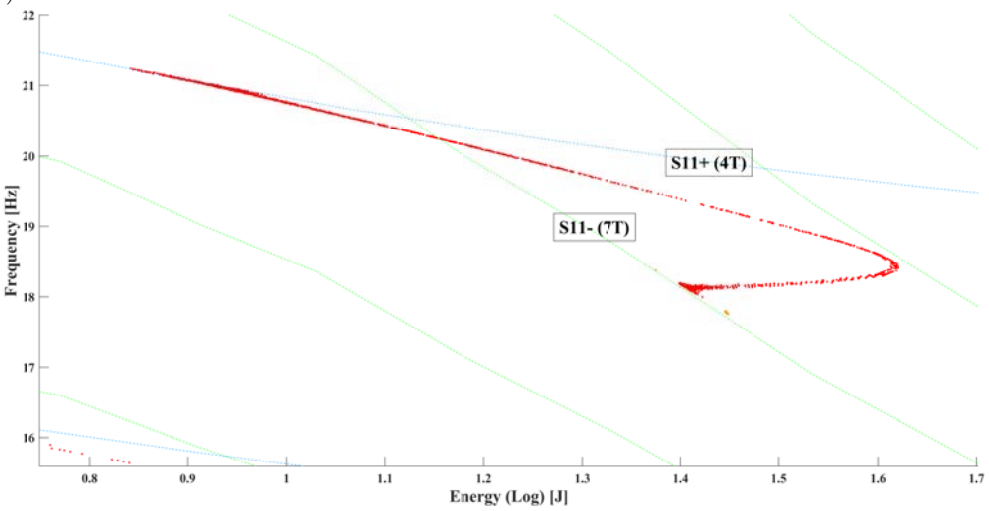

FIG. 7. Detailed illustration of a) 3:5 and b) 4:7 internal resonances.

To conclude, not only a great agreement between the results of the current approach and previous well-known methods is obvious, but also the proposed approach revealed some new bifurcations and internal resonances during the clear paths. Additionally, both could be considered to validate the proposed numerical independent approach and pave the way for investigating the dynamics of a system with more substantial nonlinearities consisting of nonlinearly elastic materials, as presented in the next section.

4. NUMERICAL INVESTIGATIONS

4.1. An elastic system with more substantial nonlinearities

After validating the proposed approach, a two-DOF system with more substantial degrading nonlinearities in all elements is considered and evaluated to demonstrate the capabilities of the independent approach. In this context, all springs are assumed to be made of elastic materials with fifth-order degrading nonlinearity, as shown in Fig. 8, where x_i indicates the displacement and m_i indicates the mass of i-th DOF, which is set equal to 4000 kg. Motion equations of the mentioned system could be formed based on the free-body diagram of each DOF, in which the inertia-based terms are related directly to absolute displacements, and the stiffness-based elements come from their corresponding relative displacements. In this context, the first step is to determine the force-displacement relation of each spring, as presented in Eq. (8):

$$\left\{ \begin{array}{l} f_{S1} = \left(2.25e13 * \Delta_1^5\right) - \left(2.8e10 * \Delta_1^3\right) + \left(1.44e7 * \Delta_1\right) \\ f_{S2} = \left(4.7e12 * \Delta_2^5\right) - \left(9.4e9 * \Delta_2^3\right) + \left(7.95e6 * \Delta_2\right) \end{array} \right\}. \tag{8}$$

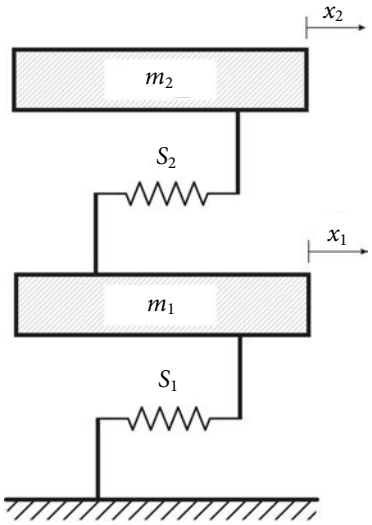

FIG. 8. Schematic illustration of springs with fifth-order degrading nonlinearity.

Furthermore, dynamical motion equations of an undamped system could be met through the free-body diagram, which is presented in Eq. (9):

$$\left\{ \begin{array}{l} f_{\text{ext}}(1) = f_I(x_1) + f_{S_1}(x_1 - 0) - f_{S_2}(x_2 - x_1) \\ f_{\text{ext}}(2) = f_I(x_2) + f_{S_2}(x_2 - x_1) + 0 \end{array} \right\}. \tag{9}$$

Afterward, by substituting (8) in (9) and considering the inertia force equal to $m_i\ddot{x}_i$, Eq. (10) shows the motion equations of the system illustrated in Fig. 8 under free vibration:

$$\left\{ \begin{array}{l} 4000\ddot{x}_1 + \left(2.25e13 * x_1^5\right) - \left(2.8e10 * x_1^3\right) + \left(1.44e7 * x_1\right) \\ \qquad + \left(4.7e12 * (x_1 - x_2)^5\right) - \left(9.4e9 * (x_1 - x_2)^3\right) \\ \qquad + \left(7.95e6 * (x_1 - x_2)\right) = 0 \\ 4000\ddot{x}_2 + \left(4.7e12 * (x_2 - x_1)^5\right) - \left(9.4e9 * (x_2 - x_1)^3\right) \\ \qquad + \left(7.95e6 * (x_2 - x_1)\right) = 0 \end{array} \right\}. \tag{10}$$

Finally, the system (10) is defined as the input of the independent approach, and the previously-mentioned coefficients are assigned to calculation variables to investigate its nonlinear dynamics.

4.1.1. Frequency-energy plot. Direct separation of the DOFs' displacements and time in motion equations is impossible due to energy-frequency dependence. Hence, the relation between frequency and energy can provide an appropriate tool to demonstrate the details of nonlinear responses during NNMs and, consequently, interpret nonlinear dynamics. To this aim, Fig. 9 illustrates the frequency of periodic responses against their corresponding total energy.

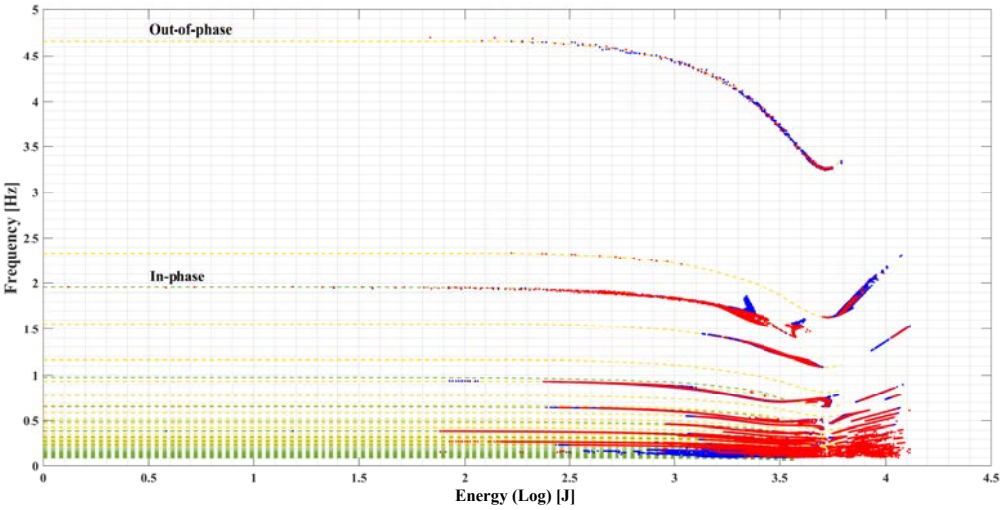

FIG. 9. Frequency-energy plot corresponding with the system (10).

Each red point indicates a periodic synchronic response and each blue point indicates a periodic non-synchronic response with a different period time value for each of the DOFs. Moreover, green and yellow dash lines are multiplications of in-phase and out-of-phase NNMs, respectively. It is worth mentioning that the starting part of each NNM during lower energies coincides with its corresponding LNM, and the decrease of frequencies over the increase of energy is due to the degrading behavior of the material's resistance. The aggregation of target points with lower frequencies could cause the data gathering to face difficulties, especially in tracking possible patterns. In this context, period-energy plot could sort out the complexities of those areas and illustrate the solutions more properly, as presented in Fig. 10.

The proximity of the NNMs' multiplications would contribute to energy exchange between them, called internal resonance. In the current problem, the most apparent internal resonances are 1:2 and 2:5, which means that the energy exchange occurs from the first multiple of in-phase NNM toward the second multiple of out-of-phase NNM for 1:2 and from the second multiple of in-phase to the fifth multiple of out-of-phase for 2:5. Figure 11 shows the mentioned internal resonances in detail.

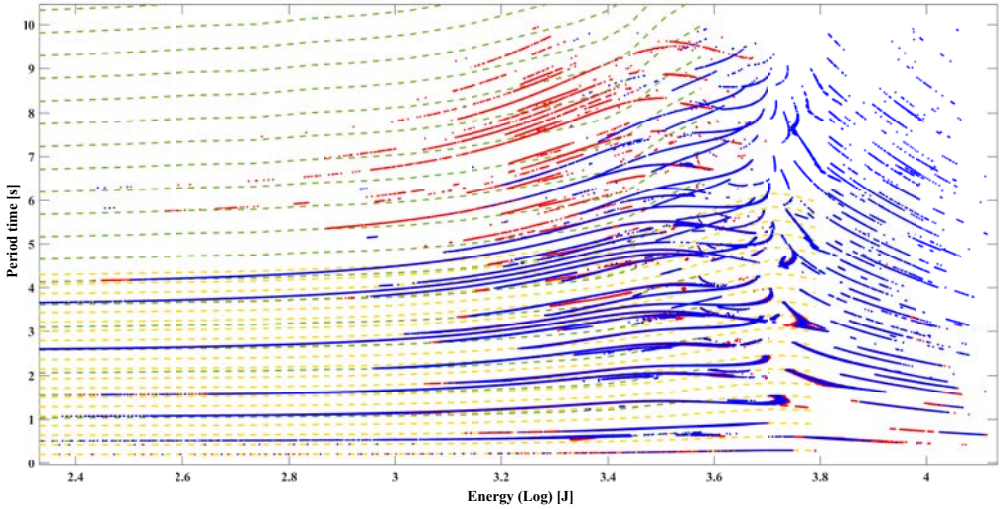

FIG. 10. Period-energy plot corresponding with the system (10).

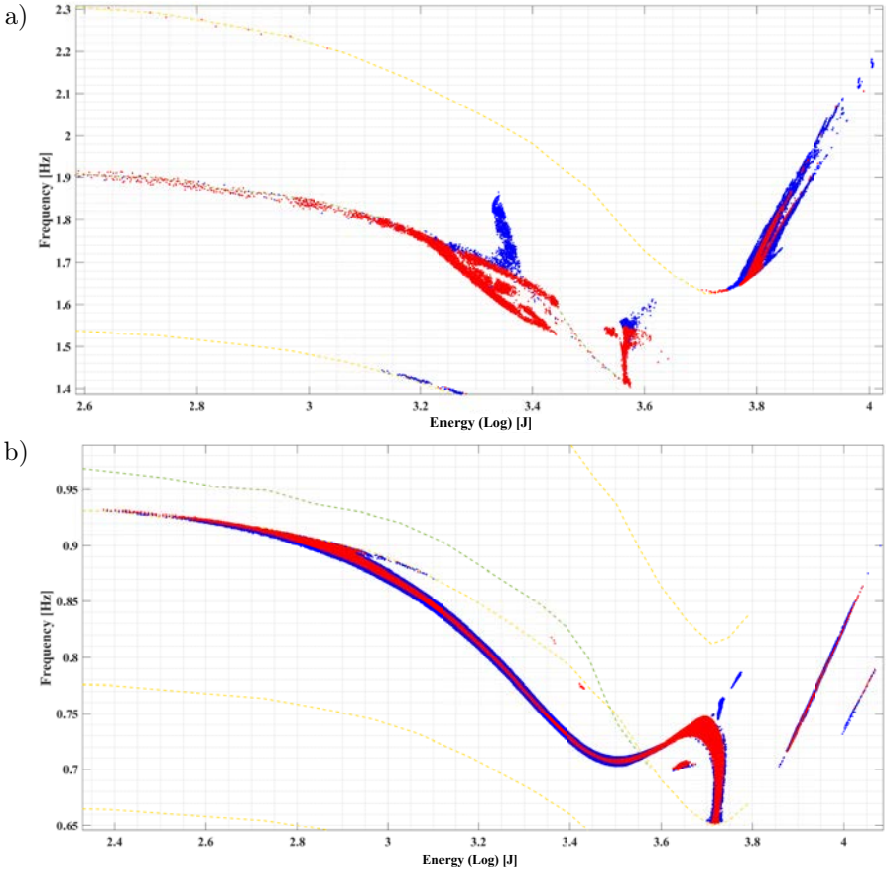

FIG. 11. Detailed illustration of a) 1:2 and b) 2:5 internal resonances.

4.1.2. Nonlinear normal modes. Classical LNMs are usually presented as rational constant numbers between DOFs, contributing to linear functions to define the relationship between those DOFs. By increasing the vibration domains of DOFs, while the system oscillates in the linear zone, the mentioned constant ratios are fixed, so the mentioned linear functions will not face any changes, and they will be sufficient to represent the LNMs of a system during the whole linear domains. However, in the nonlinear area, the relations between DOFs are not only curves, and the curves also change for different domains of DOFs. In other words, if all DOFs' displacements of a system in the nonlinear area are multiplied by a fixed number, the curves demonstrating the relation of DOFs will also be changed. The illustration of NNMs in previous studies has been limited to the modal curves of a few numbers of points on each NNM. In this paper, NNMs are separated into different sections, and modal curves of each point on each part are illustrated with respect to its corresponding energy to form a *quasi*-continuous framework. In this manner, NNMs of the initial and final parts of the out-of-phase and in-phase corresponding with the presented FEP are illustrated in Figs. 12 and 13, respectively, and *quasi*-continuous modal curves of 1:2 and 2:5 internal resonances are presented in Fig. 14. It is worth noting that 2-D projections of the first and the last NNMs are demonstrated on top of each.

4.1.3. Modal curves in phase space. Although the mentioned graphs improve the depiction of displacements relationships as indicators of each motion, the role of velocities as other variables in the initial conditions of ODEs should not be ignored, as highlighted in the invariant manifold approach. In that regard, closed modal curves in phase space are in planes tangent to the corresponding plane of LNMs at lower displacements and velocities and change to curved planes by increasing those values. In this context, by taking the displacement of the first DOF as the master coordinate, the velocities of DOFs are presented with respect to that and illustrated in Figs. 15 to 17.

4.2. A two-story steel structure with nonlinear material

To focus on more practical investigations, a full-scale experimental steel structure is employed, and its finite elements method (FEM) model is established in ABAQUS based on the dimensional details and material properties presented in [12], as shown in Fig. 18.

In the presence of nonlinear materials, the loading and unloading behaviors of the structure obey different stiffness functions, and correspondingly, the motion equations face continuously-changing stiffness components. In this context, the piecewise linearized equations illustrated in Fig. 19 fitted on hysteresis curves of both stories, which consist of a line with a slope equal to linear stiffness as the initial part, and a line with a slope equal to softened stiffness as the second part.

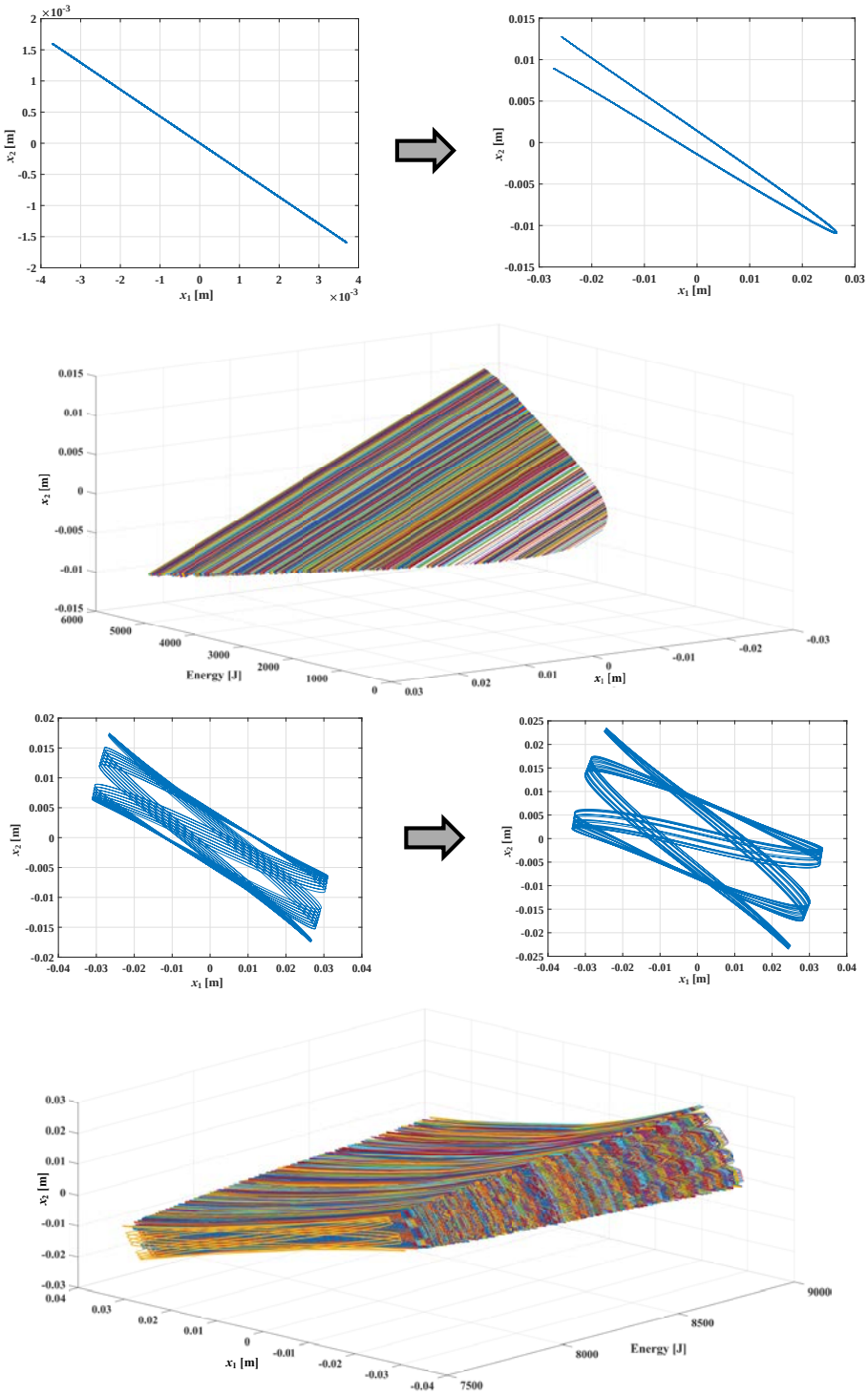

FIG. 12. NNMs of out-of-phase motion during the initial (top) and ultimate (bottom) parts.

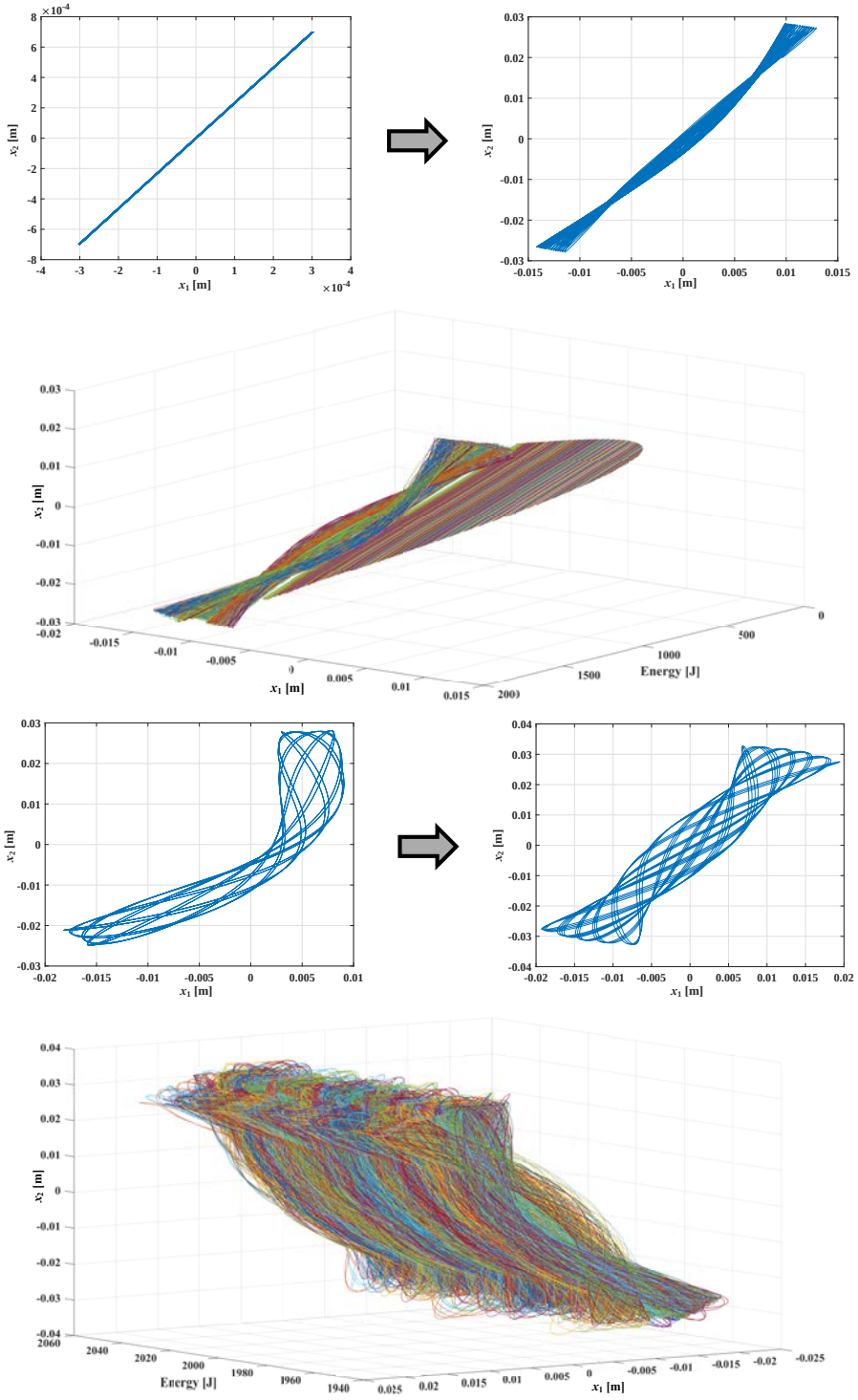

FIG. 13. NNMs of in-phase motion during the initial (top) and ultimate (bottom) parts.

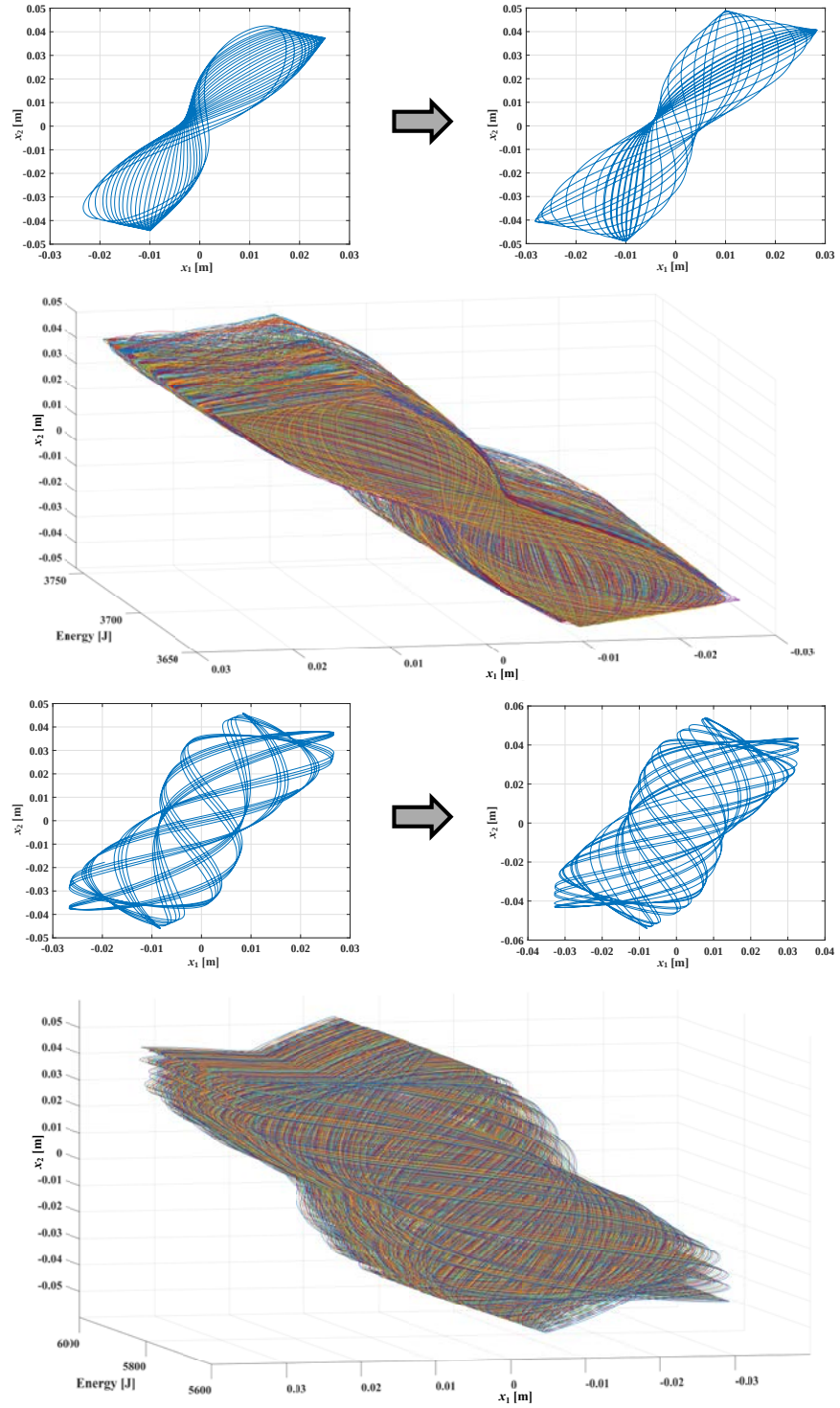

FIG. 14. NNMs of 1:2 (top) and 2:5 (bottom) internal resonances.

Afterward, the motion equations of the mentioned structure are presented in Eq. (11), where f_I indicates inertia function, f_S indicates stiffness function, X indicates displacement, $\ddot{X}$ indicates acceleration, f_{SP} indicates the force of start point on fitted hysteresis, x_{SP} indicates the displacement of start point on fitted hysteresis, $L = 1$ indicates loading state, $L = 0$ indicates unloading state, x_{intL} indicates the displacement corresponding with the intersection of two lines with different slopes during loading, x_{intU} indicates the displacement corresponding with the intersection of two lines with different slopes during unloading, and the numerical index denotes the number of DOFs:

$$\left\{\begin{array}{c} f_I(X_1) + f_{S1}(X_1 - 0) - f_{S2}(X_2 - X_1) = 0 \\ f_I(X_2) + f_{S2}(X_2 - X_1) + 0 = 0 \end{array}\right\} \rightarrow \left\{\begin{array}{c} f_{I1} = 1000\ddot{X}_1 \\ f_{I2} = 1000\ddot{X}_2 \\ f_{S1} = A_1 x_1 + B_1 \\ f_{S2} = A_2 x_2 + B_2 \end{array}\right\},$$

$$\left\{\begin{array}{l} \left\{\begin{array}{ll} A_1 = 650000, \;\; B_1 = f_{SP1} - 650000\, x_{SP1} & \\ & \text{if } L1 = 1 \text{ and } x_1 \le x_{intL1} \\ A_1 = (200000 + f_{SP1})/(0.06 + x_{SP1}), & B_1 = 200000 - A_1 0.06 \\ & \text{if } L1 = 1 \text{ and } x_1 > x_{intL1} \\ A_1 = 650000, \;\; B_1 = f_{SP1} - 650000\, x_{SP1} & \\ & \text{if } L1 = 0 \text{ and } x_1 \ge x_{intU1} \\ A_1 = (200000 - f_{SP1})/(0.06 - x_{SP1}), & B_1 = -200000 + A_1 0.06 \\ & \text{if } L1 = 0 \text{ and } x_1 < x_{intU1} \end{array}\right\} \\ \left\{\begin{array}{ll} A_2 = 650000, \;\; B_2 = f_{SP2} - 650000 x_{SP2} & \\ & \text{if } L2 = 1 \text{ and } x_2 \le x_{intL2} \\ A_2 = (200000 + f_{SP2})/(0.06 + x_{SP2}), & B_1 = 200000 - A_2 0.06 \\ & \text{if } L2 = 1 \text{ and } x_2 > x_{intL2} \\ A_2 = 650000, \;\; B_2 = f_{SP2} - 650000 x_{SP2} & \\ & \text{if } L2 = 0 \text{ and } x_2 \ge x_{intU2} \\ A_2 = (200000 - f_{SP2})/(0.06 - x_{SP}), & B_2 = -200000 + A_2 0.06 \\ & \text{if } L2 = 0 \text{ and } x_2 < x_{intU2} \end{array}\right\} \end{array}\right\}, \quad (11)$$

$$\left\{\begin{array}{l} x_{intL1} = \frac{200000 - ((200000 + f_{SP1}) * 0.06/(0.06 + x_{SP1})) - f_{SP1} + 650000 x_{SP1}}{650000 - ((200000 + f_{SP1})/(0.06 + x_{SP1}))} \\ x_{intU1} = \frac{-200000 + ((200000 - f_{SP1}) * 0.06/(0.06 - x_{SP1})) - f_{SP1} + 650000 x_{SP1}}{650000 - ((200000 - f_{SP1})/(0.06 - x_{SP1}))} \\ x_{intL2} = \frac{200000 - ((200000 + f_{SP2}) * 0.06/(0.06 + x_{SP2})) - f_{SP2} + 650000 x_{SP2}}{650000 - ((200000 + f_{SP2})/(0.06 + x_{SP2}))} \\ x_{intU2} = \frac{-200000 + ((200000 - f_{SP2}) * 0.06/(0.06 - x_{SP2})) - f_{SP2} + 650000 x_{SP2}}{650000 - ((200000 - f_{SP2})/(0.06 - x_{SP2}))} \end{array}\right\}.$$

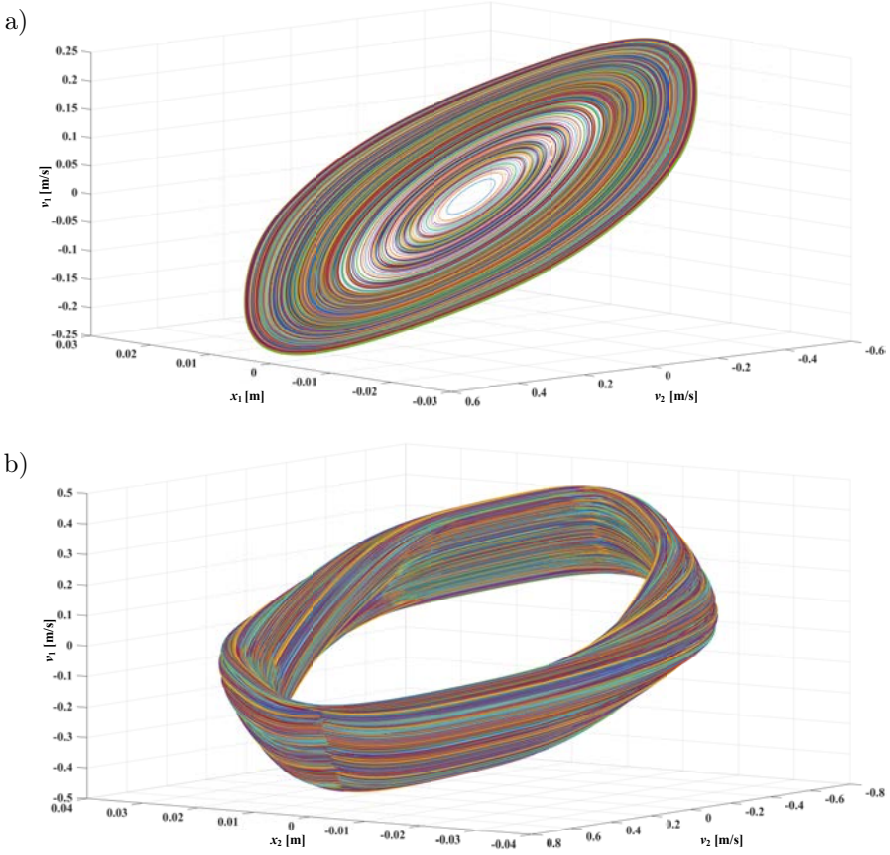

Fig. 15. Modal curves of out-of-phase motion during the initial (a) and ultimate (b) parts in phase space.

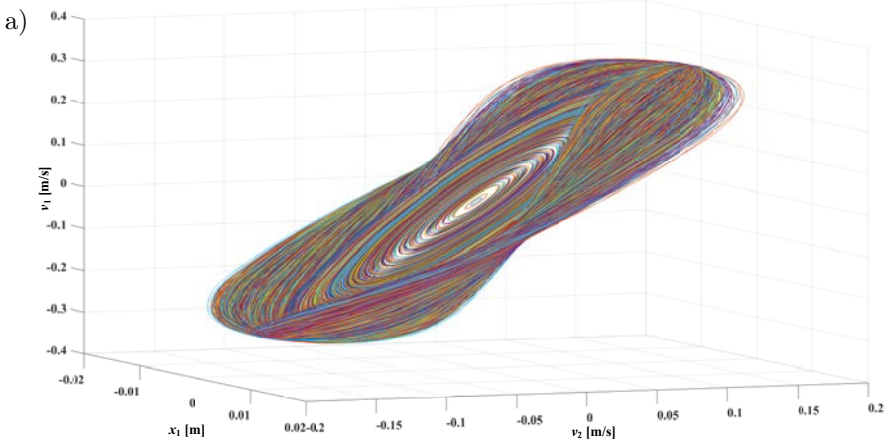

[Fig. 16a]

b)

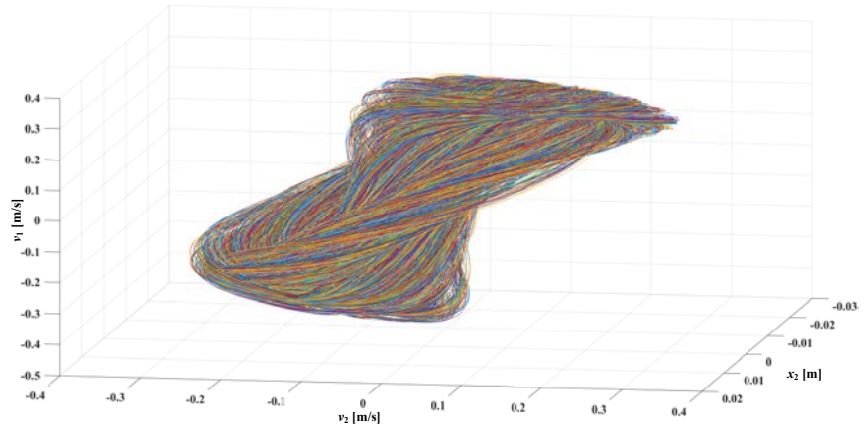

Fig. 16. Modal curves of in-phase motion during the initial (a) and ultimate (b) parts in phase space.

a)

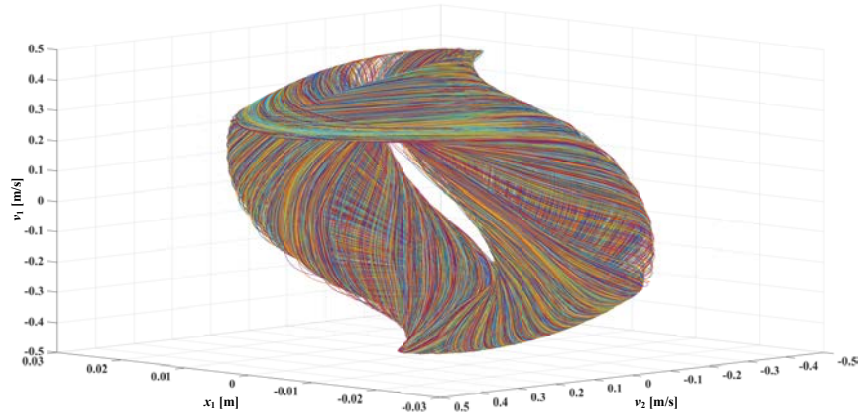

b)

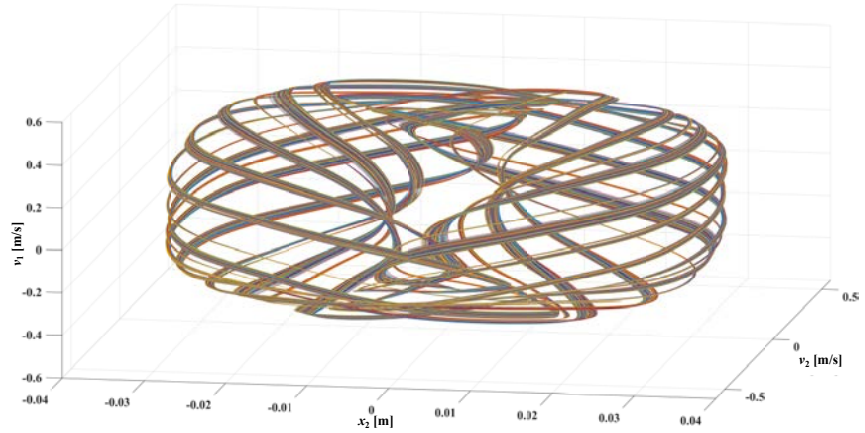

Fig. 17. Modal curves of 1:2 (a) and 2:5 (b) internal resonances in phase space.

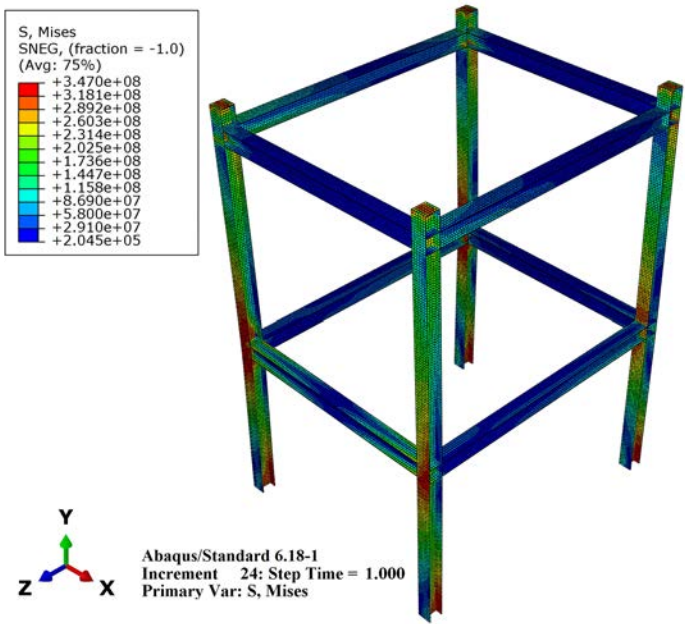

Fig. 18. FEM of the experimental steel structure studied [12].

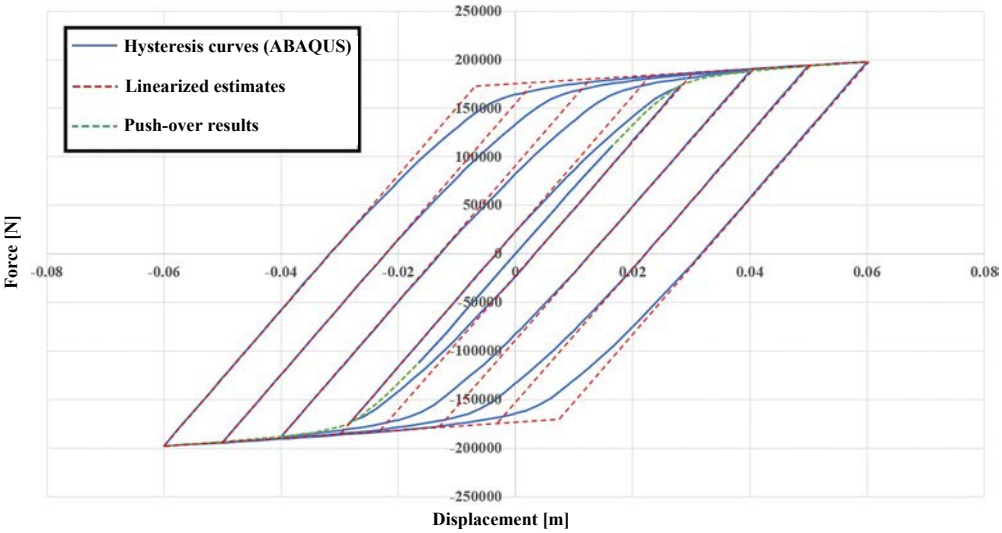

Fig. 19. Piecewise linearized equations fitted on hysteresis curves.

Finally, the FEPs corresponding with the expansion of the first and second LNMs and the close-up part of the internal resonance 1:3 are illustrated in Fig. 20. Additionally, the relationships between DOFs, namely NNMs, corre-

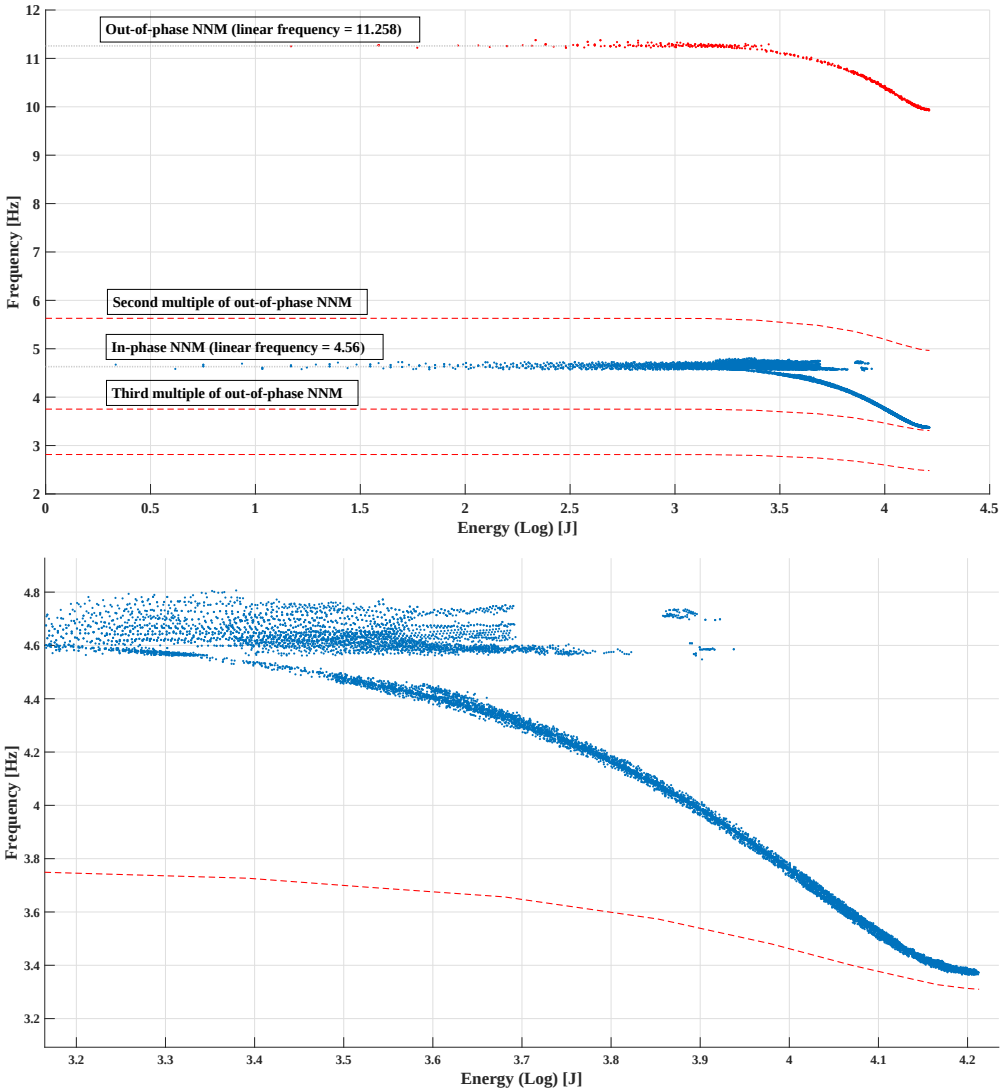

FIG. 20. FEPs corresponding with the two-story structure (top), and detailed illustration of 1:3 internal resonance (bottom).

sponding with the in-phase oscillation ($S11+$) and the mentioned internal resonance ($S13$) are presented in Fig. 21.

It is worth noting that the degradation of frequency corresponding with each NNM branch during energy increase is compatible with softening stiffness, as expected. Additionally, the presented approach for formulating the hysteresis curves by piecewise linear functions could pave the way for investigating the NNMs of structures with nonlinear materials, especially civil structures.

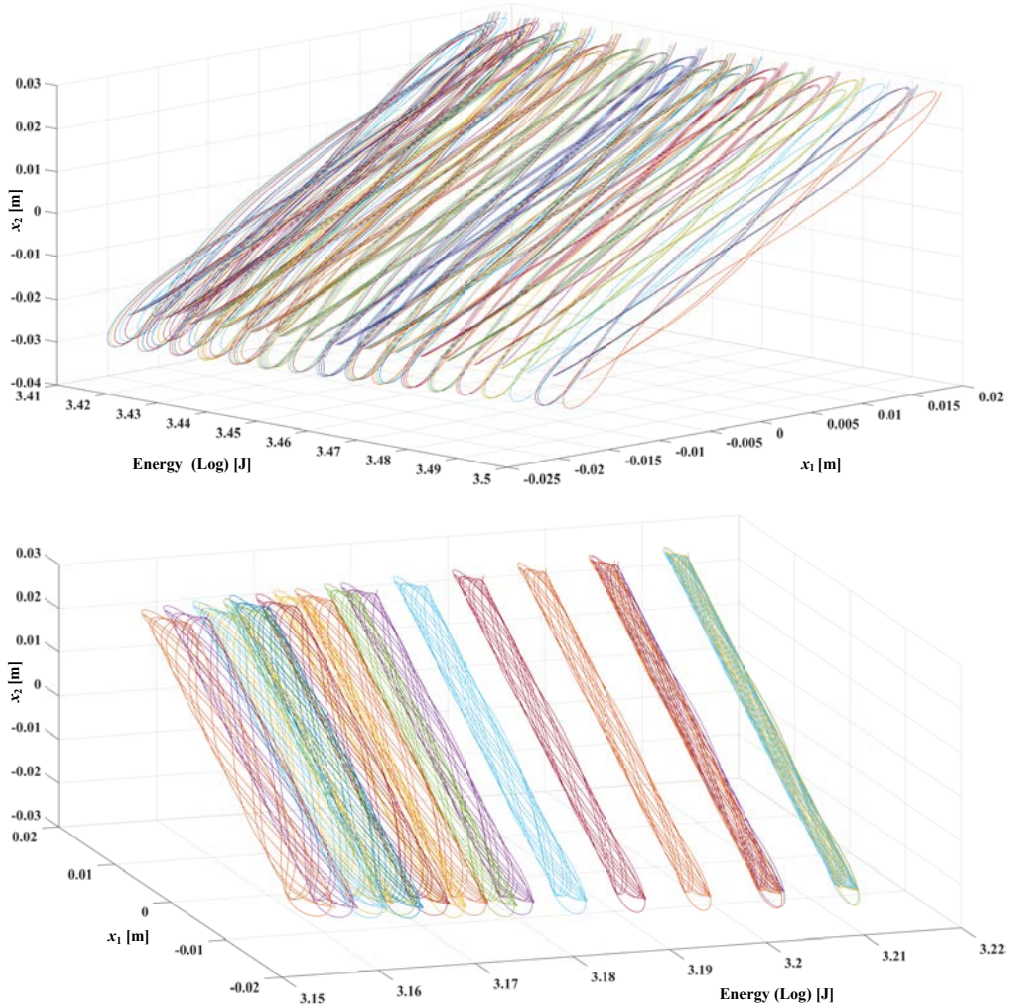

FIG. 21. NNMs of the system (11) corresponding with parts of in-phase oscillation (top) and 1:3 internal resonance (bottom).

5. Conclusion

NNMs are appropriate tools for analyzing and interpreting structures' nonlinear behavior, including various applications in nonlinear areas, such as investigating nonlinear dynamics of different real-world systems, damage detection, forming ROMs, and extracting modal characteristics. In this paper, the relation of DOFs during non-necessarily synchronic periodic oscillations was considered as the basic definition, and the periodicity algorithm was suggested to determine if an input response over time can get through the NNMs criteria, regardless of a pre-assumed period time. Afterward, a procedure was proposed to find the

NNMs from the discretized domain of the problem, which formed the independent approach. Regarding verification, after analyzing a well-known problem, great agreement was observed between the results of the current approach and the previous methods, and even some new internal resonances were obtained. Finally, an elastic system with more substantial nonlinearities and a two-story full-scale steel structure with nonlinear materials were investigated, and their corresponding FEPs and NNMs were extracted.

According to the obtained results, the system's frequency is reduced by the increase of total energy due to the decrease in resistance of nonlinear material, except during the occurrence of internal resonances. Compatibility of the results during low energies of FEP with LNMs confirms that the resulting NNMs are the nonlinear extensions of their linear counterparts. The independent approach's ability to capture bifurcations was confirmed by finding two main 1:2 and 2:5 internal resonances, which occur between different multiplications of NNMs. LNMs are like pictures with a fixed linear relation between DOFs over different energy values in linear problems. However, in nonlinear ones, NNMs as modal curves change continuously from point to point, and demonstrating them on 2-D graphs contributes to losing a portion of reality, so a video based on total energy could be a better tool to depict NNMs in detail. In this paper, the relations of different DOFs' displacements, namely NNMs, are demonstrated in a *quasi*-continuous environment over the system's total energy. Additionally, the employed approach for formulating hysteresis could pave the way for investigating the NNMs of structures with nonlinear materials, especially civil structures.

In general, the advantages of the independent approach are as follows:

- Independent from previous solutions and limiter assumptions in finding the next point.
- Covering all possible candidate solutions, even outlying ones.
- No exposure to convergence issues and uncertainties of continuous methods.
- Employing a novel periodicity checker algorithm, independent from the need for a pre-assumed period time.
- Capable of capturing all possible in-range internal resonances.

On the other hand, the relatively low speed during high resolutions could be considered as the limitation of the suggested approach. Finally, the proposed NNM-finding path is the only way to obtain a thorough investigation and clear the effects of dependence on initial assumptions. In other words, to ensure the comprehensiveness of solutions, such an approach is inevitable until the uniqueness and number of NNMs are proven theoretically. Moreover, the independent approach with higher resolutions could be employed as a reliable tool for extracting the NNMs comprehensively, and adopting lower resolutions could provide an

appropriate framework to validate the results of other approaches and case studies, especially novel ones.

References

1. A.C. Altunisik, E. Kalkan, F.Y. Okur, K. Ozgan, O. Karahasan, A. Bostanci, Nondestructive modal parameter identification of historical timber bridges using ambient vibration tests after restoration, *Measurement* (London), **146**: 411–424, 2019, doi: 10.1016/j.measurement.2019.06.051.
2. B. Bhowmik, T. Tripura, B. Hazra, V. Pakrashi, Real time structural modal identification using recursive canonical correlation analysis and application towards online structural damage detection, *Journal of Sound and Vibration*, **468**: 22 pages, 2020, doi: 10.1016/j.jsv.2019.115101.
3. E.T. Chipato, A.D. Shaw, M.I. Friswell, Nonlinear rotordynamics of a MDOF rotor–stator contact system subjected to frictional and gravitational effects, *Mechanical Systems and Signal Processing*, **159**: 107776, 2021, doi: 10.1016/j.ymssp.2021.107776.
4. T. Chujo, O. Mori, J. Kawaguchi, Normal mode analysis of rubble-pile asteroids using a discrete element method, Icarus, **321**: 458–472, 2019, doi: 10.1016/j.icarus.2018.12.011.
5. T. Detroux, L. Renson, L. Masset, G. Kerschen, The harmonic balance method for bifurcation analysis of large-scale nonlinear mechanical systems, *Computer Methods in Applied Mechanics and Engineering*, **296**: 18–38, 2015, doi: 10.1016/j.cma.2015.07.017.
6. T. Dossogne *et al.*, Nonlinear ground vibration identification of an F-16 aircraft – Part II: Understanding nonlinear behaviour in aerospace structures using sine-sweep testing, [in:] IFASD 2015 – International Forum on Aeroelasticity and Structural Dynamics, 2015.
7. E. Ellobody, Interaction of buckling modes in railway plate girder steel bridges, *Thin-Walled Structures*, **115**: 58–75, 2017, doi: 10.1016/j.tws.2016.12.007.
8. E. Ferhatoglu, E. Cigeroglu, H.N. Özgüven, A novel modal superposition method with response dependent nonlinear modes for periodic vibration analysis of large MDOF nonlinear systems, *Mechanical Systems and Signal Processing*, **135**: 106388, 2020, doi: 10.1016/j.ymssp.2019.106388.
9. M. Jahn, S. Tatzko, L. Panning-von Scheidt, J. Wallaschek, Comparison of different harmonic balance based methodologies for computation of nonlinear modes of nonconservative mechanical systems, *Mechanical Systems and Signal Processing*, **127**: 159–171, 2019, doi: 10.1016/j.ymssp.2019.03.005.
10. L. Jiang, C. Liu, L. Peng, J. Yan, P. Xiang, Dynamic analysis of multi-layer beam structure of rail track system under a moving load based on mode decomposition, *Journal of Vibration Engineering & Technologies*, **9**: 1463–1481, 2021, doi: 10.1007/s42417-021-00308-8.
11. G. Kerschen, M. Peeters, J.C. Golinval, A.F. Vakakis, Nonlinear normal modes, Part I: A useful framework for the structural dynamicist, *Mechanical Systems and Signal Processing*, **23**(1): 170–194, 2009, doi: 10.1016/j.ymssp.2008.04.002.
12. S.E. Kim, K.W. Kang, D.H. Lee, Full-scale testing of space steel frame subjected to proportional loads, *Engineering Structures*, **25**(1): 69–79, 2003, doi: 10.1016/S0141-0296(02)00119-0.

13. M.E. King, A.F. Vakakis, An energy-based formulation for computing nonlinear normal modes in undamped continuous systems, *Journal of Vibration and Acoustics, Transactions of the ASME*, **116**(3): 332–340, 1994, doi: 10.1115/1.2930433.

14. M. Krack, Nonlinear modal analysis of nonconservative systems: Extension of the periodic motion concept, *Computers and Structures*, **154**: 59–71, 2015, doi: 10.1016/j.compstruc.2015.03.008.

15. R.J. Kuether, MS. Allen, A numerical approach to directly compute nonlinear normal modes of geometrically nonlinear finite element models, *Mechanical Systems and Signal Processing*, **46**(1): 1–15, 2014, doi: 10.1016/j.ymssp.2013.12.010.

16. W. Lacarbonara, G. Rega, A.H. Nayfeh, Resonant non-linear normal modes. Part I: Analytical treatment for structural one-dimensional systems, *International Journal of Non-Linear Mechanics*, **38**(6): 851–872, 2003, doi: 10.1016/S0020-7462(02)00033-1.

17. S. Lotfan, Nonlinear modal interactions in a beam-mass system tuned to 3:1 and combination internal resonances based on correspondence between MTS and NSI methods, *Mechanical Systems and Signal Processing*, **164**: 108221, 2022, doi: 10.1016/j.ymssp.2021.108221.

18. A.M. Lyapunov, The general problem of the stability of motion, *International Journal of Control*, **55**(3): 531–534, 1992, doi: 10.1080/00207179208934253.

19. L. Meyrand, E. Sarrouy, B. Cochelin, G. Ricciardi, Nonlinear normal mode continuation through a Proper Generalized Decomposition approach with modal enrichment, *Journal of Sound and Vibration*, **443**: 444–459, 2019, doi: 10.1016/j.jsv.2018.11.030.

20. K.J. Moore, M. Kurt, M. Eriten, D.M. McFarland, L.A. Bergman, A.F. Vakakis, Time-series-based nonlinear system identification of strongly nonlinear attachments, *Journal of Sound and Vibration*, **438**: 13–32, 2019, doi: 10.1016/j.jsv.2018.09.033.

21. A. Nayfeh, R. Ibrahim, Nonlinear interactions: Analytical, computational, and experimental methods, *Applied Mechanics Reviews*, **54**(4): B60–B61, 2001, doi: 10.1115/1.1383674.

22. J.P. Nöel, L. Renson, G. Kerschen, B. Peeters, S. Manzato, J. Debille, Nonlinear dynamic analysis of an F-16 aircraft using GVT data, [in:] IFASD 2013 – International Forum on Aeroelasticity and Structural Dynamics, 2013.

23. K. Park, M.S. Allen, Quasi-static modal analysis for reduced order modeling of geometrically nonlinear structures, *Journal of Sound and Vibration*, **502**: 116076, 2021, doi: 10.1016/j.jsv.2021.116076.

24. M. Peeters, G. Kerschen, J.C. Golinval, Modal testing of nonlinear vibrating structures based on nonlinear normal modes: Experimental demonstration, *Mechanical Systems and Signal Processing*, **25**(4): 1227–1247, 2011, doi: 10.1016/j.ymssp.2010.11.006.

25. M. Peeters, R. Viguié, G. Sérandour, G. Kerschen, J.C. Golinval, Nonlinear normal modes, Part II: Toward a practical computation using numerical continuation techniques, *Mechanical Systems and Signal Processing*, **23**(1): 195–216, 2009, doi: 10.1016/j.ymssp.2008.04.003.

26. L. Renson, G. Deliége, G. Kerschen, An effective finite-element-based method for the computation of nonlinear normal modes of nonconservative systems, *Meccanica*, **49**(8): 1901–1916, 2014, doi: 10.1007/s11012-014-9875-3.

27. L. Renson, G. Kerschen, B. Cochelin, Numerical computation of nonlinear normal modes in mechanical engineering, *Journal of Sound and Vibration*, **364**: 177–206, 2016, doi: 10.1016/j.jsv.2015.09.033.

28. R.M. Rosenberg, Normal modes of nonlinear dual-mode systems, *ASME Journal of Applied Mechanics*, **27**(2): 263–268, 1960, doi: 10.1115/1.3643948.

29. R.M. Rosenberg, On nonlinear vibrations of systems with many degrees of freedom, *Advances in Applied Mechanics*, **9**(C): 155–242, 1966, doi: 10.1016/S0065-2156(08)70008-5.

30. S. Shaw, C. Pierre, Non-linear normal modes and invariant manifolds, *Journal of Sound and Vibration*, **150**(1): 170–173, 1991, doi: 10.1016/0022-460X(91)90412-D.

31. S.W. Shaw, C. Pierre, Normal modes of vibration for non-linear continuous systems, *Journal of Sound and Vibration*, **169**(3): 319–347, 1994, doi: 10.1006/jsvi.1994.1021.

32. Y. Shen, N. Béreux, A. Frangi, C. Touzé, Reduced order models for geometrically nonlinear structures: Assessment of implicit condensation in comparison with invariant manifold approach, *European Journal of Mechanics – A/Solids*, **86**: 104165, 2021, doi: 10.1016/j.euromechsol.2020.104165.

33. S. Sikdar, W. Ostachowicz, P. Kudela, M. Radzieński, Barely visible impact damage identification in a 3D core sandwich structure, *Computer Assisted Methods in Engineering and Science*, **24**(4): 259–268, 2017, doi: 10.24423/cames.187.

34. C.S.M. Sombroek, P. Tiso, L. Renson, G. Kerschen, Numerical computation of nonlinear normal modes in a modal derivative subspace, *Computers and Structures*, **195**: 34–46, 2018, doi: 10.1016/j.compstruc.2017.08.016.

35. M. Song, L. Renson, J.P. Noël, B. Moaveni, G. Kerschen, Bayesian model updating of nonlinear systems using nonlinear normal modes, *Structural Control Health Monitoring*, **25**(12): e2258, 2018, doi: 10.1002/stc.2258.

36. M. Strozzi, V.V. Smirnov, L.I. Manevitch, F. Pellicano, Nonlinear normal modes, resonances and energy exchange in single-walled carbon nanotubes, *International Journal of Non-Linear Mechanics*, **120**: 103398, 2020, doi: 10.1016/j.ijnonlinmec.2019.103398.

37. MATLAB (R2015a), The MathWorks Inc., 2015.

38. R. Walentynski, Description of large deformations of continuum and shells and their visualisation with Mathematica, *Computer Assisted Methods in Engineering and Science*, **26**(3–4): 191–209, 2019, doi: 10.24423/cames.272.

39. F. Wang, Bifurcations of nonlinear normal modes via the configuration domain and the time domain shooting methods, *Communications in Nonlinear Science and Numerical Simulation*, **20**(2): 614–628, 2015, doi: 10.1016/j.cnsns.2014.06.008.

40. B. Xu *et al.*, Nonlinear modal interaction analysis and vibration characteristics of a Francis hydro-turbine generator unit, *Renewable Energy*, **168**: 854–864, 2021, doi: 10.1016/j.renene.2020.12.083.

41. L. Xu, Y. Hui, W. Zhu, X. Hua, Three-to-one internal resonance analysis for a suspension bridge with spatial cable through a continuum model, *European Journal of Mechanics – A/Solids*, **90**: 104354, 2021, doi: 10.1016/j.euromechsol.2021.104354.

42. Q. Zhao, T. Han, D. Jiang, K. Yin, Application of variational mode decomposition to feature isolation and diagnosis in a wind turbine, *Journal of Vibration Engineering and Technologies*, **7**(6): 639–646, 2019, doi: 10.1007/s42417-019-00156-7.

Received February 23, 2022; revised version August 31, 2022;
accepted August 31, 2022.